ACS OMEGA

http://pubs.acs.org/journal/acsodf

Article

Reduction−Magnetic Separation of Pickling Sludge by Biomass Pyrolysis Reducing Gas

Yane Xu, Yuanfeng Shu, Yichao Wang, Xiaoling Ren, Xinqian Shu,* Xize Zhang, Huiyun Song, Huixin Zhou, Lingwen Dai, Zhipu Wang, Xiang Yuan, and Hongyu Zhao

Cite This: *ACS Omega* 2022, 7, 17963−17975

Read Online

ACCESS | Metrics & More | Article Recommendations

ABSTRACT: The neutralization process of carbon steel pickling wastewater produces a large amount of steel hydrochloric acid pickling sludge (SHPS), and improper treatment of this sludge poses a serious threat to the environment. Considering that SHPS contains a large amount of iron oxide and given the huge demand for iron concentrate in China's ironmaking industry, refining iron oxide in SHPS into iron concentrate will have great environmental and economic benefits. This paper proposes a new method that uses biomass (corncob) to replace conventional coal-based reductants for the recovery of iron components in SHPS to simultaneously utilize two kinds of solid waste resources. Factors that affect the iron recovery rate and iron grade of SHPS, such as the reaction temperature, corncob dosage, residence time, and magnetic field strength, were studied using a fixed bed and a magnetic separator. These studies were combined with thermodynamic analysis, thermogravimetric analysis, X-ray diffraction, inductively coupled plasma−mass spectrometry, gas chromatography, etc. The results showed that when the reaction temperature was 680 °C, the corncob dosage was 5%, the residence time was 20 min, and the magnetic field strength was 200 mT, the recovery rate of iron reached 91.83%, and the iron grade of the recovered products was 67.72%, meeting the level I requirements in GB/T 32545-2016. Based on this result, a process involving SHPS reduction roasting with corncob pyrolysis reducing gas−magnetic separation was established to recover iron from SHPS. This process not only effectively utilizes the iron oxide in SHPS by converting it into iron concentrate powder for the ironmaking industry but also proves that the pyrolysis gas of corncob has good reduction ability.

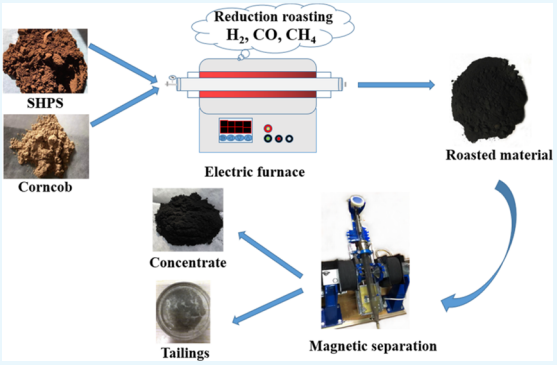

1. INTRODUCTION

Carbon steel is a widely used and versatile material. During carbon steel production and processing, an oxide layer is formed, and this oxide layer reduces the corrosion resistance of steel. At present, the most common surface treatment for carbon steel strips is pickling, which uses hydrochloric acid to remove the oxide layer. This method produces a large amount of pickling wastewater, which is highly acidic and contains large amounts of heavy metal ions and chloride. Therefore, the wastewater must be treated before being discharged. Lime or caustic soda neutralization is recognized as one of the most effective heavy metal wastewater disposal methods for some small- and medium-sized carbon steel surface treatment plants, but it produces a large amount of heavy metal-containing steel hydrochloric acid pickling sludge (SHPS), which contains chlorine. According to statistical reports, the annual output of SHPS in China in recent years has exceeded 500 000 tons.[1] SHPS exhibits leaching toxicity, pollutes soil and water, can cause chromosomal aberrations in plants, and causes potential harm to human health.[2−4] In China, as per the National List of Hazardous Waste (2021 version),[5] SHPS is hazardous waste, so it is urgently necessary to develop treatment, management, and disposal technologies for SHPS.

The conventional approach for treating SHPS is landfilling, which often follows stabilization/solidification. Increasingly stringent environmental and landfill regulations coupled with the increasing costs of raw materials make it imperative to find a feasible method of recycling and treating SHPS to replace the traditional landfill method. Some theoretical and experimental studies have been performed on utilizing SHPS resources. The utilization methods studied include making bricks[6,7] and glass ceramics,[8] preparing P-doped polyferric chloride coagulants,[9] and preparing spinel ferrite.[10] However, when SHPS is used for building materials such as bricks or ceramics, the amount of SHPS added is limited and the metals in SHPS still exist in the

Received: March 3, 2022
Accepted: May 9, 2022
Published: May 18, 2022

https://doi.org/10.1021/acsomega.2c01122
ACS Omega 2022, 7, 17963−17975

Figure 1. (a) Corncob before crushing, (b) corncob after being dried and crushed through a 150 μm sieve, (c) SHPS before crushing, and (d) SHPS after being dried and crushed through a 150 μm sieve.

building materials; these materials have not been effectively utilized as resources and involve a risk of leaching into the environment under specific environmental conditions.[6,7] The process of preparing iron-based coagulants takes a long time.[9] The market demand for the production of ferrite is very limited.

However, SHPS is an inevitable product in the carbon steel industry and contains a large amount of Fe_2O_3. Effectively utilizing the Fe contained in SHPS in the modern ironmaking industry is a highly attractive strategy to solve the problems related to the depletion of high-grade iron ores. The traditional method to improve the iron grade of an iron ore is to reduce weakly magnetic Fe_2O_3 to strongly magnetic Fe_3O_4 with a coal-based reducing agent and then separate the strongly magnetic Fe_3O_4 and nonmagnetic components in the roasted material by magnetic separation. However, coal-based reductants usually need a high reduction temperature, so some researchers have used alternatives, such as biomass, to replace coal-based reducing agents.

Biomass not only has good reducing agent characteristics but also has the advantages of a large number of resources, low price, and renewability. To date, there have been some relevant studies on reducing iron oxide with biomass instead of coal-based reducing agents. For example, Rath et al.[11] explored the application of biomass briquette that was produced from unused vegetative remnants as an alternative reductant for the reduction roasting−magnetic separation of an iron ore slime sample with 56.2% Fe. Their findings showed that iron ore concentrates with ∼65% Fe and ∼64% weight recovery were obtained with reduction conditions including a temperature of 650−750 °C, a reductant-to-feed ratio of 0.15, a residence time of 30−45 min, and a reductant size of −3 + 1 mm. Wei et al.[12] studied the reducing reaction characteristics of the chemical reagent hematite (Fe_2O_3% >99%) with the main biomass components, and the reduction kinetics of iron oxide by lignin (a main component of biomass) were also studied. Zhao et al.[13] found that in a double-layer reactor, under a pyrolysis temperature of 600 °C in the lower layer and a catalytic reforming temperature of 650 °C in the upper layer, when the volatiles produced by the copyrolysis of lignite and corn straw penetrated into the upper catalyst bed composed of an iron ore, almost all Fe_2O_3 peaks in the iron ore disappeared and Fe_3O_4 peaks appeared after catalytic reforming of the volatiles by the iron ore. Their research results confirm that in this process, a natural iron ore can catalyze and reform the volatiles that are produced by the copyrolysis of lignite and corn straw, and the reducing gases (CO and H_2) produced by pyrolysis can also react with the iron ore to produce CO_2 and Fe_3O_4 in a double-layer reactor. This reduced iron can be used as a high-quality raw material for ironmaking. Kurniawan et al.[14] studied the effect of combined coal−biomass with various biomass blending ratios (BBRs) on coal−biomass-integrated copyrolysis−tar decomposition over a low-grade iron ore, and the highest carbon content of a porous iron ore (4.70%) was obtained when BBR-25% was used. These studies show that in the temperature range of 600−700 °C, the reductive volatilization produced by biomass pyrolysis can effectively reduce Fe_2O_3 to Fe_3O_4. The required reduction temperature is approximately 200 °C lower than the overall temperature of bituminous coal, which is necessary to reduce Fe_2O_3.[15] Under medium- and low-temperature conditions, the apparent activation energy of biomass pyrolysis is lower than that of bituminous coal pyrolysis. Although some studies on biomass-based reduction of iron oxide have been carried out, there is a lack of literature on biomass-based reduction of SHPS. Therefore, it is of great significance to explore the reduction and magnetization of SHPS by biomass pyrolysis for solid waste recycling, energy conservation, and emission reduction and to improve the ecological environment.

Among many forms of agricultural and forestry waste biomass, corncob has the advantages of easy grinding, easy storage and transportation, large output, and wide distribution. However, there is no literature on the reduction of iron oxide by corncob instead of traditional coal-based reductants. Therefore, this article innovatively selects corncob as a biomass reducing agent to verify whether the reducing gas produced by corncob pyrolysis can effectively reduce iron oxides in SHPS under

https://doi.org/10.1021/acsomega.2c01122
ACS Omega 2022, 7, 17963−17975

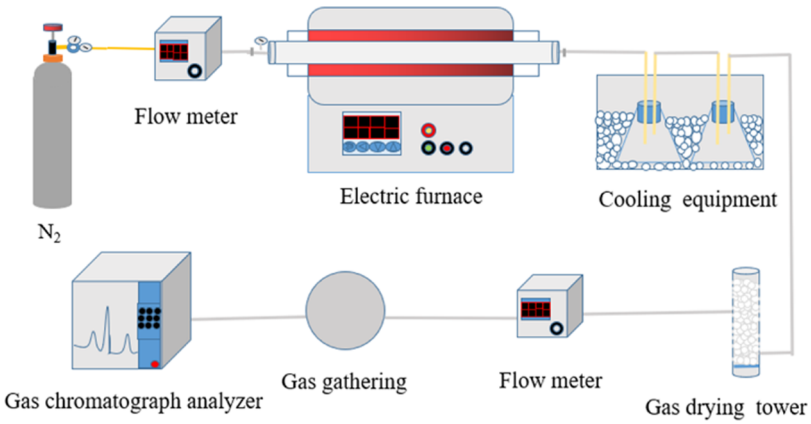

Figure 2. Configuration of the apparatus for the pyrolysis−reduction roasting experiment.

appropriate experimental conditions. Considering the above-mentioned facts, the present study aims to explore the possibility of the application of biomass (corncob) in the reduction roasting of a Chinese SHPS sample containing Fe_2O_3 to recover iron from SHPS; the goal of this recovery process is to effectively utilize SHPS as a resource and alleviate the supply shortage of iron concentrate powder, as well as to establish a new bioreductant (corncob) that will function as an alternative to coal in the future and broaden the resource utilization channels of the corncob. First, the characteristics (including appearance, chemical composition, elemental and industrial analysis, scanning electron microscopy (SEM) microstructure, X-ray diffraction (XRD) crystal phase, and thermogravimetric (TG) properties) of SHPS and corncob were analyzed. Then, the pyrolysis characteristics of the corncob were studied to clarify the temperature range and concentration of reducing gas emitted by corncob pyrolysis. Furthermore, the Gibbs free energy of the reaction of reducing components such as CO, H_2, CH_4, and C with Fe_2O_3 in SHPS at different reaction temperatures was studied by thermodynamic calculations. Finally, the effects of the reaction temperature, corncob addition amount, residence time, and magnetic separation intensity on the Fe recovery ratio and Fe grade in SHPS were studied using a fixed bed and magnetic separation tube. This research provides a new idea for the recovery and utilization of SHPS and corncob.

2. MATERIALS AND METHODS

2.1. Preparation of SHPS and Corncob Samples. The SHPS sample was supplied by a steel surface processing plant (Tianjin City, China). The corncob sample was collected from a farm in a suburb of Tianjin City. The SHPS powder and corncob were crushed into fine particles and sieved such that only particles less than 150 μm in diameter were utilized. Figure 1 presents photographs of the SHPS and corncob samples.

2.2. Characterization Techniques. Different integrated instrumental characterization studies were carried out for the reductant (corncob), SHPS sample, and roasted and magnetic separation products. The O, N, and H contents in the ultimate analysis of the samples were analyzed by an American Leco ONH863 analyzer, while C and S were analyzed by an American Leco CS844 analyzer. The proximate analysis of the samples was carried out on an American Leco TGA801 industrial analyzer.

The elemental content (except chlorine) of the samples was tested using an Agilent ICP−MS 7700 instrument. The chlorine content in the powder samples was analyzed using an ARL AdvantX Intellipower TM3600 X-ray fluorescence spectrometer (Thermo Fisher). X-ray diffraction (XRD) patterns of the samples were obtained with a Rigaku D/Max 2500 (Japan) X-ray diffractometer utilizing a Cu Kα radiation source to determine the crystalline phases. Scanning electron microscopy (SEM) images were recorded by a Zeiss Sigma 300 (Germany) scanning electron microscope to observe the morphology.

TG analysis was carried out using a synchronous STA 8000 thermal analyzer (PerkinElmer). To preheat the reaction system and evacuate the air in the reaction chamber, the circulating water pump was opened before the beginning of the experiment, and 100 mL/min argon was injected at the same time. When the system temperature was stable and the carrier gas pressure was constant at 2 MPa, approximately 8−10 mg of dried experimental sample was placed in a prefired ceramic crucible. The heating rate for TG analysis was 15 °C/min, and the final temperature was 950 °C.

2.3. Experimental Methods: Pyrolysis−Reduction Roasting and Magnetic Separation. All reduction roasting experiments were conducted in an electric furnace. Figure 2 shows a schematic diagram of the experimental device during pyrolysis−reduction roasting. A total of 10 g of an SHPS sample was thoroughly mixed with the desired amount of the corncob and stored in a quartz tube. Before each test, high-purity N_2 with a flow rate of 40 mL/min was injected into the quartz tube to maintain an inert atmosphere for the reactions. After roasting for the required time, the samples were removed and cooled with N_2. The roasted mass was ground to a −150 μm size and subjected to magnetic separation using a low-intensity magnetic separator with a magnetic field intensity of 0−400 mT. The strongly magnetic and nonmagnetic fractions were collected separately, dried, and analyzed for total iron (Fe(T)) content, and the iron recovery rate was calculated. The strongly magnetic fraction was regarded as the product. The experimental process flow is presented in Figure 3.

In the pyrolysis experiment of the corncob without SHPS, after the pyrolysis reaction was completed and the sample had cooled to room temperature, the coke product was collected and weighed. The pyrolysis tar was collected with dichloromethane and then distilled through a rotary evaporator, and the masses of bio-oil and water were calculated. The gas products were collected in an air bag, and then the volume fractions of the main small-molecule reducing gases were analyzed by gas chromatography (Shjinmi GC112a).

The product yield of corncob pyrolysis was calculated as follows

https://doi.org/10.1021/acsomega.2c01122
ACS Omega 2022, 7, 17963−17975

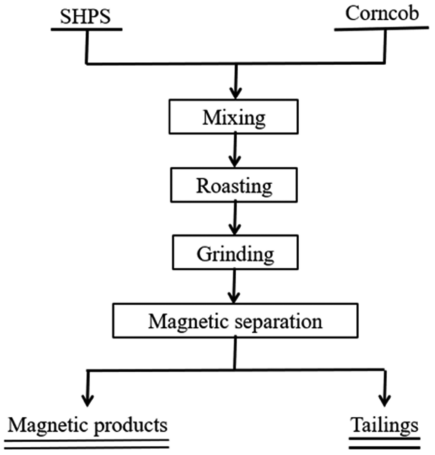

Figure 3. Flowchart of SHPS reduction.

$$Y_1 = \frac{m_1}{m} \times 100\% \quad (1)$$

$$Y_2 = \frac{m_2}{m} \times 100\% \quad (2)$$

$$Y_3 = \frac{m_3}{m} \times 100\% \quad (3)$$

$$Y_4 = 100 - Y_1 - Y_2 - Y_3 \quad (4)$$

where Y_1, Y_2, Y_3, and Y_4 are the yields of pyrolysis char, tar, water, and gas, respectively, and m_1, m_2, m_3, and m are the masses of the char, tar, water, and feedstock, respectively.

2.4. Statistical Design. The recovery rates of Fe in the strongly magnetic concentrates were calculated according to mass balance. The formula used to calculate the recovery rate is as follows

$$\text{recovery rate} = \frac{M_1 \times \omega_1}{M_2 \times \omega_2} \times 100\% \quad (5)$$

Note: M_1— quantity of strongly magnetic concentrate, g; ω_1—grade of iron in concentrate, %; M_2—quantity of the raw material, g; and ω_2—grade of iron in the raw material, %.

2.5. Analysis of SHPS and Corncob Characteristics. The chemical composition of the SHPS sample is shown in Table 1. As shown in Table 1, SHPS contains large amounts of Ca, Cl, and Fe (~30%), and Fe is one of the main raw materials in the iron and steel industry, can be well separated, and has a great recovery value.

The ultimate and proximate analyses of the corncob and SHPS are presented in Table 2. The results of the ultimate analysis presented in Table 2 show that the C content of SHPS was 2.38%; this C mainly comes from the organic acid mist inhibitor that was added to prevent HCl gas from escaping during the steel pickling process.[16,17] The relatively low content of C indicates that it is difficult for SHPS to burn. The H content was only 1.94%, which indicates that there are few hydrogen-rich aliphatic side chains in SHPS and that SHPS has a low calorific value. The moisture content in SHPS was 13.38%, the ash content was 77.14%, and the volatile content was 4.65%. The high ash content further indicates that SHPS has a low calorific value during combustion and a low organic matter content. As shown in Table 2, the C content in the corncob reached 43.62%, and the content of H was 5.98%, while the proximate analysis showed that the volatile content reached 76.16%; therefore, corncob has the potential to produce volatile reducing gas by pyrolysis to reduce iron oxide in SHPS.

Figure 4 shows the results of SEM analysis of the external characteristics of the corncob and sludge. The microstructure of the corncob shown in Figure 4a consists of long strips embedded with pores, and this structure is conducive to the release of volatile compounds during pyrolysis. As shown in Figure 4b, SHPS has a microscopic structure consisting of bright and fluffy irregular spheres and dark and very small irregular particles,[18] and the structure of the sludge is complicated.

To determine the phases in the SHPS sample, an XRD analysis was performed, as shown in Figure 5. In addition, Figure 5 shows that Fe in SHPS generally exists in the form of a trivalent iron oxide, which is weakly magnetic and cannot easily be recycled. Furthermore, the diffraction peak in the diffraction pattern of SHPS is complex, which means that this material is difficult to recycle without treatment.

3. RESULTS AND DISCUSSION

3.1. Thermogravimetric Analysis and Pyrolysis Characteristics of the Corncob. Figure 6 shows the TG-derivative thermogravimetry (DTG) curves of the high-temperature behavior of the SHPS and corncob samples. A mass loss of approximately 15.09% was observed for SHPS in the temperature range of 100−900°C. The weight loss at 50−150 °C was mainly caused by the desorption of physically adsorbed water and adsorbed gas, and the weight loss at 200−400°C was mainly caused by the dehydroxylation of a small amount of aqueous minerals, such as goethite (formula 6), in SHPS.[19,20] The weight loss at 260−950 °C was mainly caused by the thermal decomposition of a small amount of organic matter and calcium carbonate in SHPS.[21]

$$2Fe(OH)_3 \rightarrow Fe_2O_3 + 3H_2O \quad (6)$$

When the temperature was 100−260 °C, the mass reduction rate of corncob remained basically unchanged; there was basically no thermal decomposition reaction at this stage, and the composition of the corncob remained basically unchanged. When the pyrolysis temperature was greater than 260 °C, the TG curve began to decline rapidly, indicating that volatile compounds were released. There was a second trough in the DTG curve near 290 °C, and the release rate of volatiles reached the maximum at this point. The TG curve shows that the weight loss rate of the corncob was very small after 500 °C, indicating that the pyrolysis reaction tends to become stable when the pyrolysis temperature of the corncob exceeds 500 °C. The residual mass of the corncob decreased from 94.84−22.68% in the range of 260−500 °C, which was attributed to the complex composition of the corncob. A corncob contains cellulose and

Table 1. Chemical Composition of SHPS

	chemical composition (%)											
sample	Fe	Zn	Mn	Ca	Na	K	Mg	Si	Al	Cl	P	S
SHPS	29.80	0.02	0.29	11.11	3.38	0.005	0.19	4.78	0.21	12.13	0.01	0.02

https://doi.org/10.1021/acsomega.2c01122
ACS Omega 2022, 7, 17963−17975

Table 2. Ultimate and Proximate Analysis of the SHPS and Corncob Samples

	ultimate analysis (ad) wt (%)					proximate analysis (ad) wt (%)			
sample	C	H	O	N	S	M	V	A	FC
SHPS	2.38	1.94	17.30	0.19	0.37	13.38	4.65	77.14	4.82
corncob	43.62	5.98	49.88	0.51	0.01	4.21	76.16	2.75	16.88

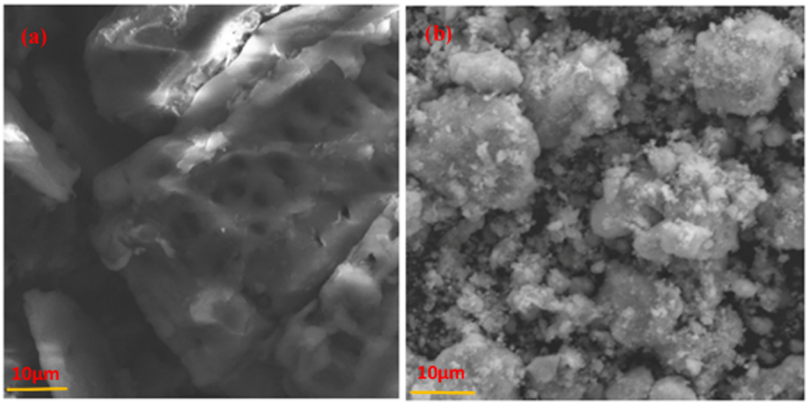

Figure 4. Scanning electron micrographs of the crushed corncob (a) and SHPS (b).

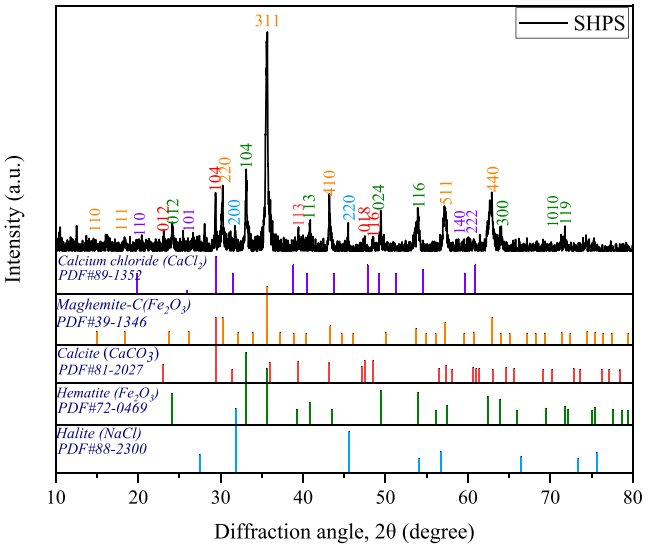

Figure 5. XRD diffraction pattern of the SHPS sample.

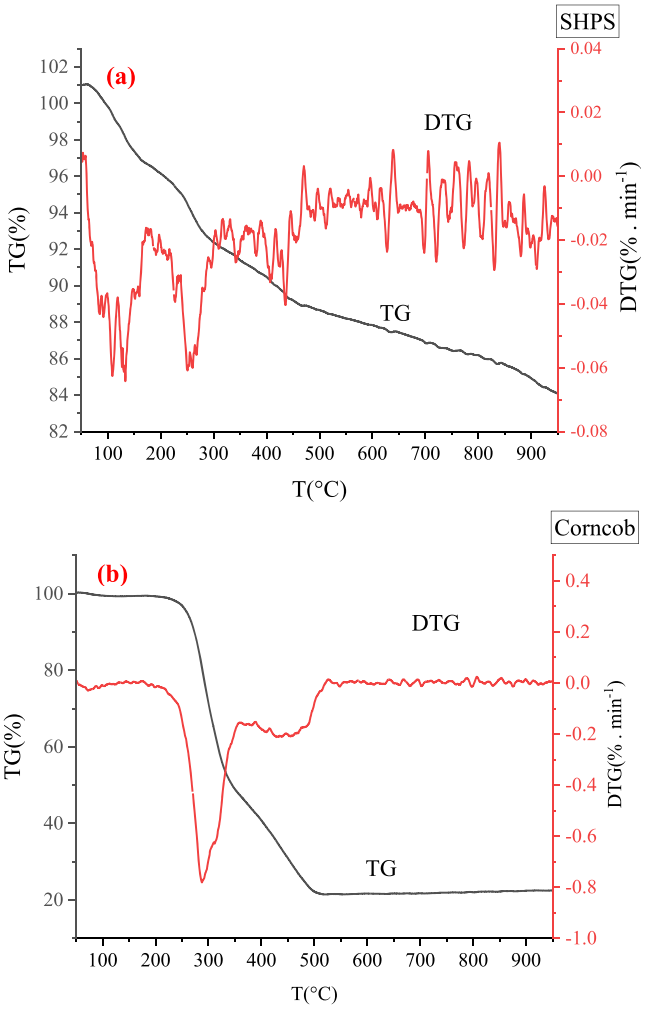

Figure 6. TG/DTG profiles of SHPS (a) and the corncob (b) after drying at 105 °C.

hemicellulose, which are connected by weak bonds. In this temperature range, the bonds in the corncob were easily broken, generating a large amount of volatiles and resulting in a significant decrease in weight.[22] The temperature range of 300−325 °C mainly involved the decomposition of hemicellulose and a small amount of lignin, and at 340−375 °C, the degradation of cellulose predominated.[23] After the experiment, the mass fraction of residual carbon was 22.48%. Additionally, the corncob had a higher mass loss than SHPS because the corncob contains a higher content of volatile matter, as shown in Table 2.

The corncob (10 g) was dried and sieved to 150 μm and the temperature was increased to 300, 400, 500, 600, 700, 800, and 900 °C in a tubular pyrolysis furnace, as shown in Figure 2, at a heating rate of 15 °C/min. Gas samples were collected in a collection bag at intervals of 100 °C from 300 to 900 °C, and the gas composition was analyzed by gas chromatography. After being maintained at the desired temperature for 40 min, the residue was removed and cooled to room temperature. The distribution of the pyrolysis products obtained is shown in Table 3, and Figure 7a shows the change trends for the four pyrolysis

https://doi.org/10.1021/acsomega.2c01122
ACS Omega 2022, 7, 17963−17975

Table 3. Dependence of Corncob Product Yields on Pyrolysis Temperature

temperature (°C)	char (wt %)	gas (wt %)	oil (wt %)	water (wt %)
300	31	33	15	21
400	30	34	16	20
500	27	35	22	16
600	25	37	23	15
700	26	41	16	17
800	24	42	14	20
900	22	43	13	22

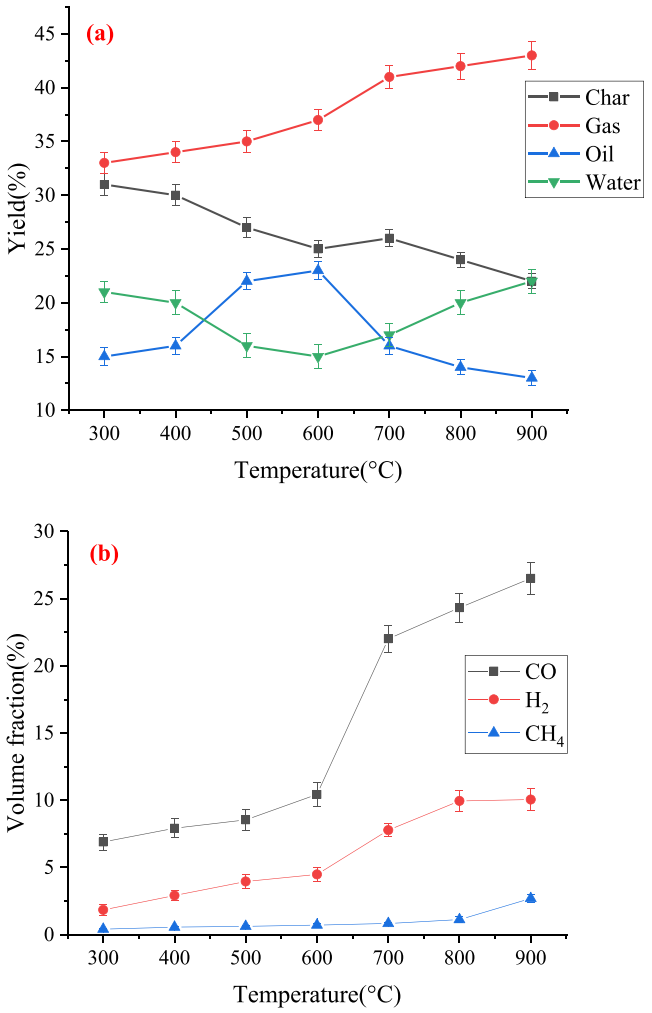

Figure 7. Yield of corncob pyrolysis products at different pyrolysis temperatures (a) and volume fractions of small-molecule reducing gases in corncob pyrolysis gas (b).

product phases of the corncob obtained at different pyrolysis temperatures. As shown in Figure 7a, corncob pyrolysis generates biomass char, biomass oil, water, and gas, and the gas yield increases with temperature after a moderate temperature. As shown in Table 3, the proportion of gas-phase pyrolysis products increased from 33 to 43% from 300 to 900 °C. This is because a thermal path that led to the formation of mainly oils and chars at low and moderate temperatures was replaced by a thermal reaction that led to the formation of additional gas at higher temperatures. If the temperature is increased, particularly to 600 °C or more, the reaction rate increases, and long-chained compounds break down into smaller compounds. This process can be explained by the fact that the gaseous yield is higher during the transition from 600 to 900 °C than for other temperature intervals, as shown in Figure 7a.

The volume fraction of the main small-molecule reducing gases at different pyrolysis temperatures is shown in Table 4, and

Table 4. Volume Proportions of Small-Molecule Reducing Gases Produced by the Corncob at Different Pyrolysis Temperatures

temperature (°C)	CO (vol %)	H_2 (vol %)	CH_4 (vol %)
300	6.89	1.84	0.41
400	7.92	2.91	0.56
500	8.54	3.96	0.62
600	10.43	4.48	0.71
700	22.01	7.78	0.83
800	24.32	9.95	1.12
900	26.51	10.05	2.69

Figure 7b shows the corresponding change trends. As shown in Figure 7b and Table 4, the yield of small-molecule reducing gases increased with increasing temperature, especially above 600 °C. CH_4 in the pyrolysis gas mainly comes from the cracking of aliphatic side chains.[24] CO mainly originates from the decomposition of oxygen-containing functional groups, and the yield of CO was higher than that of H_2 and CH_4, which indicated that the corncob contained a relatively high content of oxygen. The gas from corncob pyrolysis originates not only from the primary pyrolysis process but also from the secondary thermal cracking of volatile compounds.[25,26] These pyrolysis reducing gases provide reducing agents for the medium- and low-temperature reduction of iron oxide in SHPS.

3.2. Thermodynamic Analysis. To investigate the ability of reducing gases in corncob pyrolysis gas to reduce iron oxide in SHPS, the change law of the Gibbs free energy for the reaction between the gas components and SHPS at different reduction temperatures was calculated by thermodynamic analysis. After the sample is dried, Fe is mainly present as an oxide. Therefore, the thermodynamic analysis in this paper mainly examines the reaction of Fe_2O_3 with multiple reducing substances. When the pyrolysis temperature is 600 °C, the main reducing components in corncob pyrolysis gas are approximately 4.48 vol % H_2, 0.71 vol % CH_4, and 10.34 vol % CO. According to the relevant species of reactants and products, the possible chemical reaction between pyrolysis gas and Fe_2O_3 is shown in eqs 7−18. As a comparative study, this paper also calculates the reduction thermodynamic data for coal series reductants. When using a coal series reductant, the main reduction medium is fixed carbon; the main reduction reaction is shown in eqs 19−22. According to the thermodynamic calculation method (listed in eqs 7−22; the calculation formula of $\Delta_r G_m^{\theta}(T)$ is $\Delta_r G_m^{\theta}(T) = \Delta_r H_m^{\theta}$ (298.15 K) − $T\Delta_r S_m^{\theta}$ (298.15K), where $\Delta_r H_m^{\theta}$ (298.15 K) and $\Delta_r S_m^{\theta}$ (298.15 K) are based on Schedule 1 (i.e., thermodynamic data for selected substances) from "Inorganic Chemistry" (5th edition) compiled by the Department of Inorganic Chemistry of Dalian University of Technology.[27]), the standard reaction Gibbs free energy change ($\Delta_r G^{\theta}$m, kJ/mol) of each reaction varies with temperature, as shown in Figure 8. Thermodynamically, $\Delta_r G_m^{\theta} > 0$ means that a chemical reaction cannot occur; on the contrary, when $\Delta_r G_m^{\theta} < 0$, the reaction will spontaneously occur, and the more negative the $\Delta_r G_m^{\theta}$ value is, the more easily the reaction takes place.[28]

https://doi.org/10.1021/acsomega.2c01122
ACS Omega 2022, 7, 17963−17975

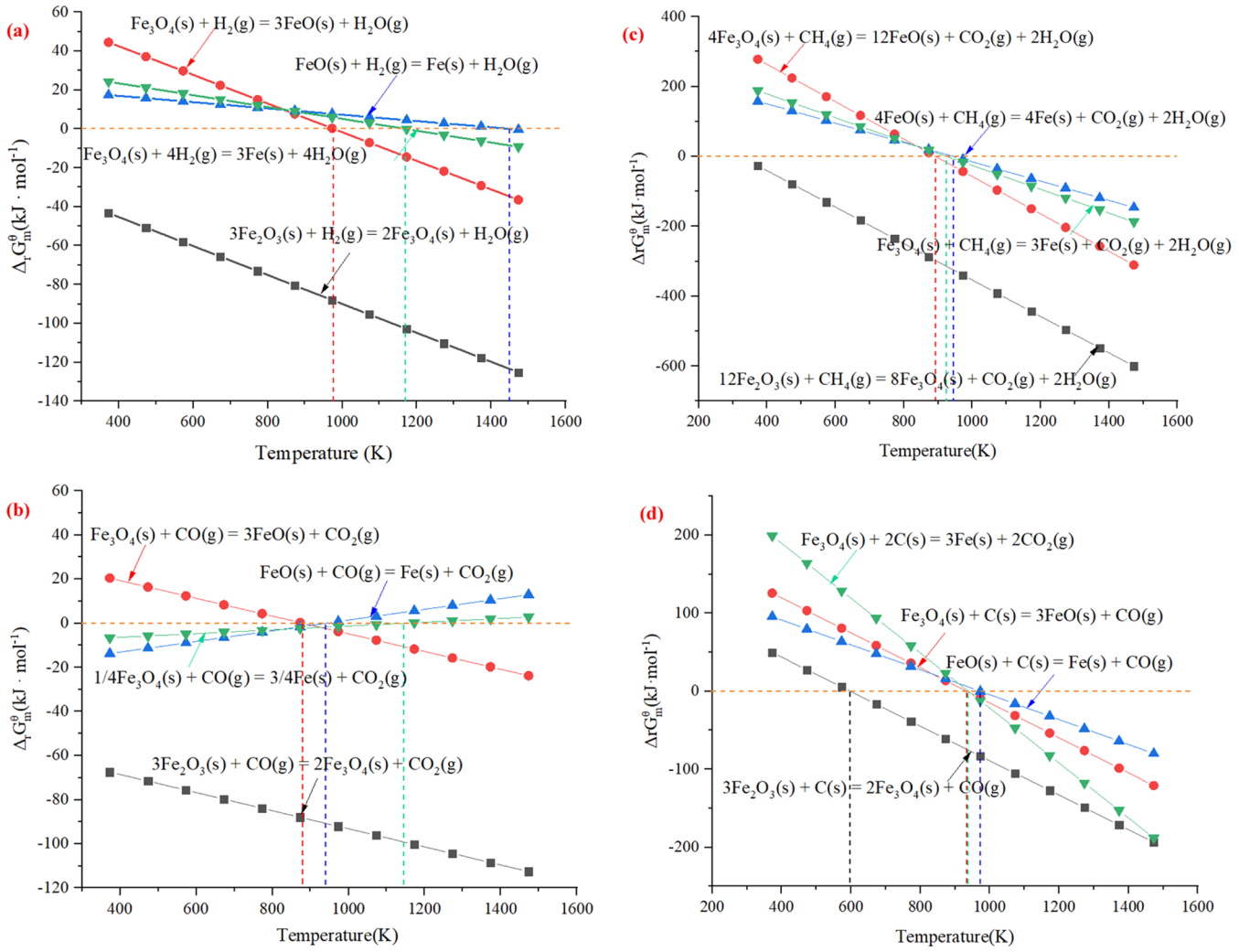

Figure 8. Change in standard reaction Gibbs free energy against temperature for the reaction of iron oxides with H_2 (a), CO (b), CH_4 (c), and C (d).

$$3Fe_2O_3(s) + H_2(g) = 2Fe_3O_4(s) + H_2O(g),\ \Delta_r G_m^\theta = -15\,547 - 74.40T,\ J/mol \quad (7)$$

$$Fe_3O_4(s) + H_2(g) = 3FeO(s) + H_2O(g),\ \Delta_r G_m^\theta = 71\,940 - 73.62T,\ J/mol \quad (8)$$

$$FeO(s) + H_2(g) = Fe(s) + H_2O(g),\ \Delta_r G_m^\theta = 23\,430 - 16.16T,\ J/mol \quad (9)$$

$$Fe_3O_4(s) + 4H_2(g) = 3Fe(s) + 4H_2O(g),\ \Delta_r G_m^\theta = 35\,550 - 30.40T,\ J/mol \quad (10)$$

$$3Fe_2O_3(s) + CO(g) = 2Fe_3O_4(s) + CO_2(g),\ \Delta_r G_m^\theta = -52\,131 - 41.00T,\ J/mol \quad (11)$$

$$Fe_3O_4(s) + CO(g) = 3FeO(s) + CO_2(g),\ \Delta_r G_m^\theta = 35\,380 - 40.16T,\ J/mol \quad (12)$$

$$FeO(s) + CO(g) = Fe(s) + CO_2(g),\ \Delta_r G_m^\theta = -22\,800 + 24.26T,\ J/mol \quad (13)$$

$$1/4Fe_3O_4(s) + CO(g) = 3/4Fe(s) + CO_2(g),\ \Delta_r G_m^\theta = -9832 + 8.58T,\ J/mol \quad (14)$$

$$CH_4(g) + 12Fe_2O_3 = 8Fe_3O_4 + CO_2(g) + 2H_2O(g),\ \Delta_r G_m^\theta = -167\,906 - 521.27T,\ J/mol \quad (15)$$

$$4Fe_3O_4 + CH_4(g) = 12FeO + CO_2(g) + 2H_2O(g),\ \Delta_r G_m^\theta = 477\,307 - 534.60T,\ J/mol \quad (16)$$

https://doi.org/10.1021/acsomega.2c01122
ACS Omega 2022, 7, 17963−17975

$$4FeO + CH_4(g) = 4Fe + CO_2(g) + 2H_2O(g),\ \Delta_r G_m^\theta = 261\,012 - 276.24T,\ J/mol \quad (17)$$

$$Fe_3O_4 + CH_4(g) = 3Fe + CO_2(g) + 2H_2O(g),\ \Delta_r G_m^\theta = 315\,085 - 340.83T,\ J/mol \quad (18)$$

$$3Fe_2O_3(s) + C(s) = 2Fe_3O_4(s) + CO(g),\ \Delta_r G_m^\theta = 132\,028 - 220.85T,\ J/mol \quad (19)$$

$$Fe_3O_4(s) + C(s) = 3FeO(s) + CO(g),\ \Delta_r G_m^\theta = 209\,379 - 224.18T,\ J/mol \quad (20)$$

$$FeO(s) + C(s) = Fe(s) + CO(g),\ \Delta_r G_m^\theta = 155\,305 - 159.59T,\ J/mol \quad (21)$$

$$Fe_3O_4(s) + 2C(s) = 3Fe(s) + 2CO_2(g),\ \Delta_r G_m^\theta = 330\,359 - 351.836T,\ J/mol \quad (22)$$

As shown in Figure 8, when the temperature is in the range of 273.00−1400.00 K, the standard reaction Gibbs free energies of eqs 7, 11, and 15 are always negative ($\Delta_r G_m^\theta < 0$), indicating that Fe_2O_3 in SHPS is easily reduced to Fe_3O_4 by H_2, CO, and CH_4. The standard Gibbs free energies of eqs 7, 11, and 15 decrease as the temperature increases, which means that increased temperature can promote the reduction magnetization of Fe_2O_3. The Gibbs free energy of eq 19 is generally positive ($\Delta_r G_m^\theta > 0$) below 600 K, which indicates that the reduction of Fe_2O_3 by carbon-based reductants requires a higher reduction temperature than does the reduction of Fe_2O_3 by reducing gas.[29] This is consistent with the research results of Sohn and Freehan, which confirmed that compared to reduction by reducing gas, reduction by carbon was negligible at and below 900 °C.[30] However, when the temperature exceeded 1000 K, weakly magnetic FeO was produced, and the recovery rate of the product was reduced. Therefore, to ensure that the reduction product is strongly magnetic, the reaction temperature should theoretically be below 1000 K. The composition of SHPS is complex, the biomass pyrolysis reduction process may be affected by various factors, and the theoretical analysis may differ from the actual reaction, so we need to comprehensively investigate the influencing factors of the reduction−magnetic separation process.

3.3. Effect of Pyrolysis Temperature on the Recovery Index. The mass ratio of SHPS to corncob was 96:4%, the final pyrolysis temperature was 400−800 °C, and the residence time after the final temperature was reached was 10 min. The solid pyrolysis residue of SHPS was magnetically separated with a 250 mT magnetic field intensity in a magnetic separator. The effect of pyrolysis temperature on the Fe recovery rate and Fe grade of the concentrate is shown in Figure 9.

Figure 9 shows that the reduction temperature had a strong influence on the iron grade and recovery ratio. When the temperature was 680 °C, the reduced iron grade and recovery ratio were the highest and reached 67.31 and 92.42%, respectively. When the reduction temperature was lower than 680 °C, the Fe grade and recovery ratio increased gradually with

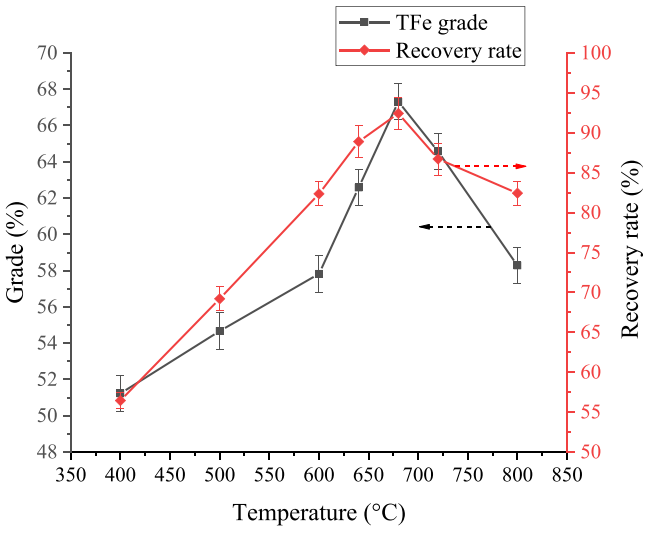

Figure 9. Effect of pyrolysis temperature on the recovery index.

increasing reaction temperature. With increasing reaction temperature, the volatile content of small-molecule reducing gas produced by corncob pyrolysis also increased after volatile decomposition;[31] thus, the conversion rate of Fe_2O_3 to Fe_3O_4 was accelerated. This is consistent with the phenomenon in Figure 6b, which shows that when the temperature increased to 260−600 °C, two large weight loss peaks of corncob appeared, indicating that the main reducing gases were released. According to the thermodynamic analysis (Figure 8), the Gibbs free energy of the reaction of CO, H_2, and CH_4 with Fe_2O_3 decreases significantly with increasing temperature, which is conducive to the reduction of Fe_2O_3 to Fe_3O_4. When the temperature exceeds 680 °C, on the one hand, too high a temperature causes SHPS to experience local sintering, and the reducing atmosphere cannot fully contact Fe_2O_3 in SHPS, which reduces the reduction rate of SHPS; on the other hand, according to the thermodynamic analysis (Figure 8), the Gibbs free energy of the reaction between CO, H_2, and Fe_3O_4 is less than 0 at 600 and 700 °C, indicating that the higher content of reducing gases such as CO and H_2 from corncob pyrolysis can deeply reduce part of the SHPS into weakly magnetic wustite (FeO),[32] reducing the Fe grade and recovery rate of SHPS. In addition, when the temperature is too high, Fe_2O_3 may react with Na_2O and CaO to form $2CaO{\cdot}Fe_2O_3$, and $Na_2O{\cdot}Fe_2O_3$,[33] which will also reduce the grade and recovery ratio of iron. In addition, if the temperature is too high, the reduction roasted material is sintered, and the reduction conditions deteriorate.[34,35] Therefore, the roasting temperature should be maintained at approximately 680 °C.

3.4. Effect of Biomass Addition on the Recovery Index. Further experiments were performed to investigate the effect of the biomass addition amount on SHPS Fe_2O_3 reduction and recovery. Corncob dosages of 1, 2, 3, 4, 5, 6, and 7 wt % were used in reduction experiments at 680 °C for 10 min. The magnetic field strength was 250 mT. Figure 10 shows variation in the recovery index with the corncob addition amount.

As shown in Figure 10, the Fe recovery rate and grade were greatly affected by the amount of biomass added. As the amount of the corncob increased, the reduced iron grade and recovery ratio showed a trend of first increasing and then decreasing. When the addition ratio was less than 5 wt %, the iron oxide in the sludge could not be fully reduced, and the recovery rate was

https://doi.org/10.1021/acsomega.2c01122
ACS Omega 2022, 7, 17963−17975

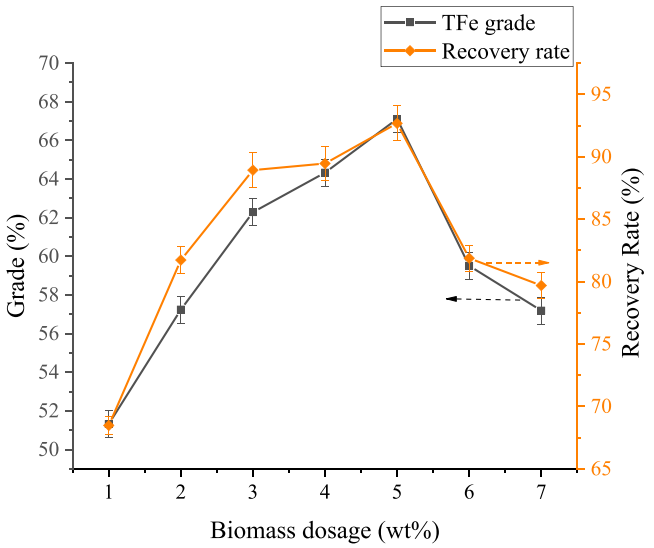

Figure 10. Effect of the biomass addition ratio on the recovery index.

low. When 5 wt % corncob was added, the grade and recovery rate of the product increased significantly, reaching 67.39 and 92.68%, respectively, and the magnetic separation index was better. With a further increase in corncob addition, the grade and recovery rate began to decrease, which may be due to a large amount of reducing volatiles being produced by excessive corncob quantities, leading to overreduction; as a result, weakly magnetic wustite (FeO) formed, which reduced the magnetic separation recovery. In addition, pickling sludge contains a large amount of alkali metals, which easily reduce the ash melting temperature of corncob and lead to agglomeration.[15] When the amount of corncob is large, the impurities in the product increase,[15] and the Fe grade decreases. Therefore, the appropriate amount of corncob was 5 wt %.

3.5. Effect of Residence Time on the Recovery Index. The amount of the corncob used was 5 wt %, and the particle size was less than 150 μm; at 680 °C, the particle size of SHPS was less than 150 μm, and the magnetic field strength was 250 mT. The magnetization effect of SHPS in the 5−35 min time range is shown in Figure 11. As shown in Figure 11, the residence time

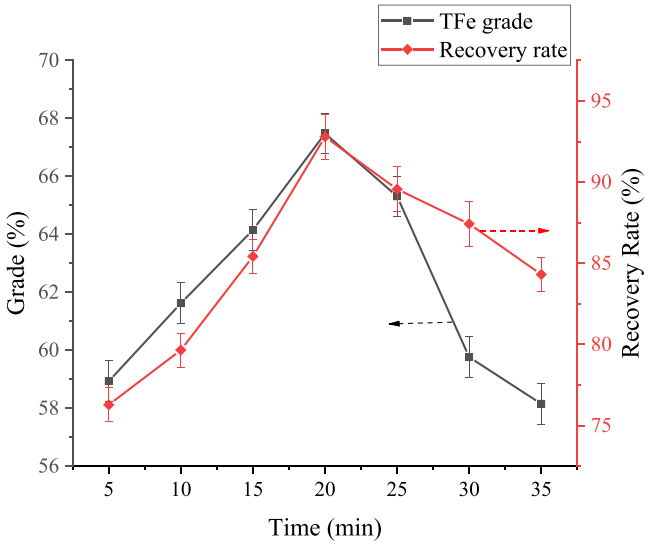

Figure 11. Effect of residence time on the recovery index.

had a great influence on the SHPS magnetization effect; SHPS magnetization increased more obviously with increasing residence time. Before a residence time of 20 min, the total Fe grade and recovery rate increased significantly. After 20 min, the Fe grade decreased significantly, and the recovery showed a gradual downward trend. Therefore, when the temperature reaches 680 °C, the appropriate residence time should be set to 20 min.

3.6. Effect of the Magnetic Field Strength on the Recovery Index. The influence of magnetic field intensity on the recovery index is shown in Figure 12 under the following

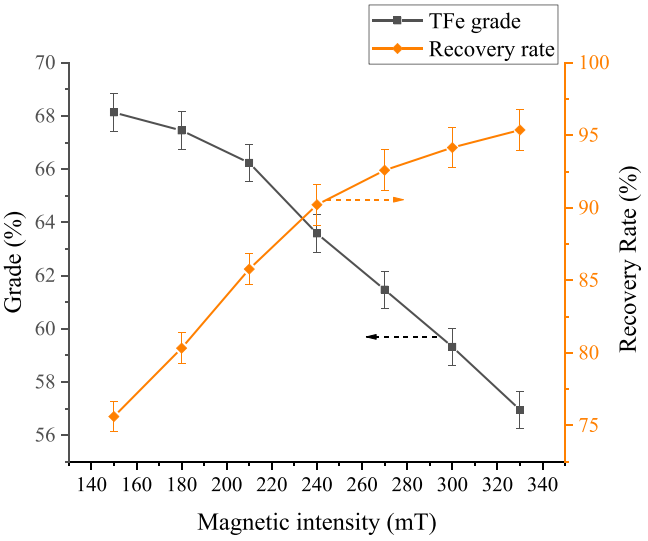

Figure 12. Effect of magnetic field intensity on the recovery index.

conditions: 5 wt % corncob, at 680 °C for 20 min, and a roasted product particle size of less than 150 μm. With increasing magnetic field intensity, the change trends of the iron grade and recovery rate were opposite. When the magnetic field intensity increased from 150 to 300 mT, the recovery rate nearly linearly increased from 87.83 to 92.93%, while the iron grade of the product decreased from 67.95 to 67.26%. When the magnetic field intensity is too low, the recovery rate is low.[36] When the magnetic field intensity is too high, some weak magnetic substances may be adsorbed, and some undissociated impurities can be trapped, resulting in an increase in the recovery rate and a decrease in the Fe grade of the recovered products. When the magnetic field intensity was 200 mT, the Fe grade and recovery rate were 67.72 and 91.83%, respectively. Choosing the appropriate magnetic field intensity can not only realize the recovery of magnetic materials but also save energy. In this paper, 200 mT was selected as the magnetic field intensity for magnetic separation of the reduction product.

In summary, the optimized conditions were a reaction temperature of 680 °C, a corncob dosage of 5%, a N_2 atmosphere, a residence time of 20 min, a roasted product particle size of less than 150 μm, and a magnetic field strength of 200 mT. Under these conditions, the recovery rate of Fe reached 91.83%, and the grade of Fe reached 67.72%.

3.7. Characterization of the Products Obtained under the Optimum Conditions. The XRD spectrum of the recovered product from the optimized conditions is shown in Figure 13. Compared with the original SHPS (Figure 5), almost all of the Fe_2O_3 peaks in the roasted material disappeared, and Fe_3O_4 peaks appeared instead. The impurities in the magnetic

https://doi.org/10.1021/acsomega.2c01122
ACS Omega 2022, 7, 17963−17975

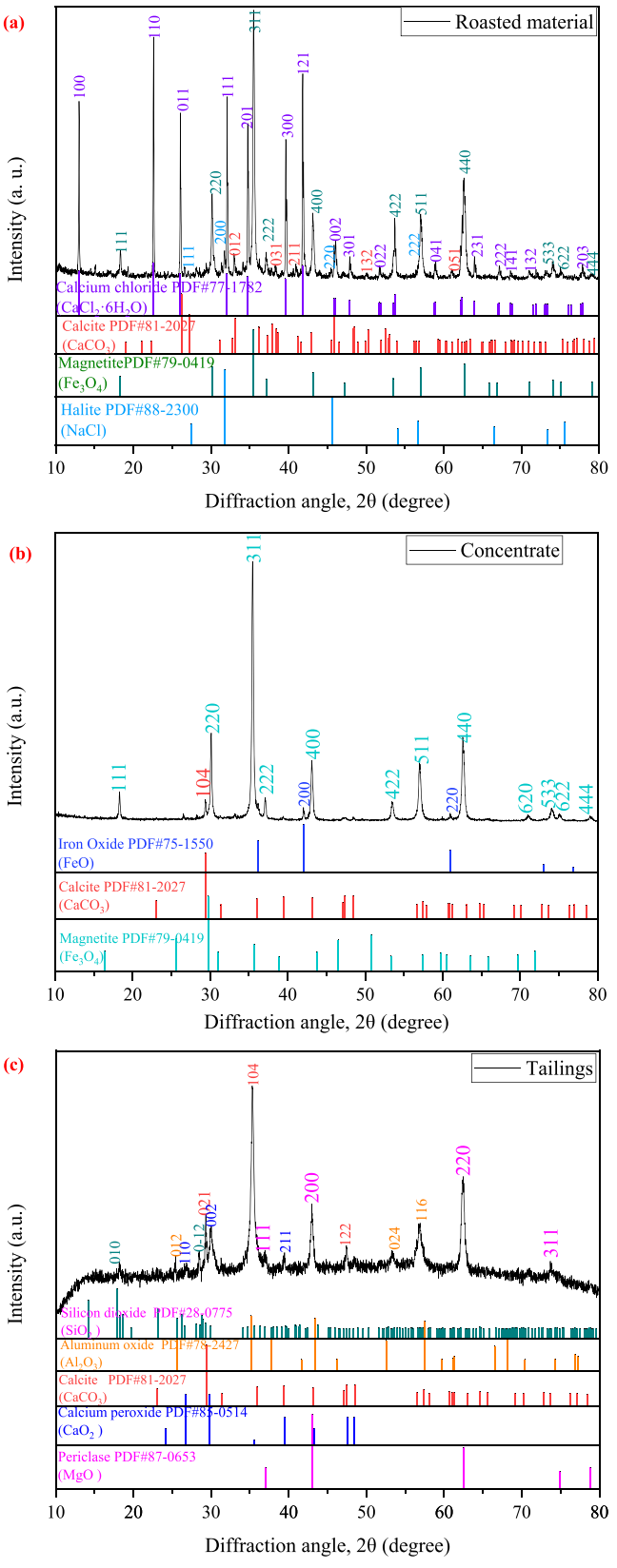

Figure 13. XRD diffraction patterns of the roasted material (a), concentrate (b), and tailings (c).

concentrate product are significantly reduced, and the main component is Fe_3O_4. The tailings mainly consisted of non-magnetic components, such as $CaCO_3$, SiO_2, and Al_2O_3.

Figure 14 shows photos of the roasted material, concentrate, and tailings. Figure 14 shows that after reduction roasting of SHPS is performed, the color of the product is notably different from the red color of the SHPS raw material. The roasted material and concentrate are black, while the tailings are light gray.

Table 5 shows the main components of the concentrate product; the total content of Fe in the product reached 67.72%. Compared with the values in Table 1, the content of Cl in the concentrate decreased from 12.13 to 0.39% after roasting–magnetic separation, and the contents of Na, Ca, and K also decreased significantly because these three elements in SHPS mostly combined with Cl to form water-soluble chlorides. Most of these chlorides were dissolved in an aqueous solution during wet magnetic separation, and only a small amount remained in the concentrate. The filtrate produced by wet magnetic separation is mainly saline liquid containing soluble chlorine salt, and this part of the filtrate should be recycled after water treatment, such as pretreatment—microfiltration—reverse osmosis—evaporative crystallization. Table 6 shows the classification of the magnetite concentrated in GB/t 32545-2016.[37]

Table 6 shows that the grade of Fe in the magnetic separation concentrate obtained under the selected experimental conditions reached the level I requirements in GB/T 32545-2016. In addition to the magnetic separation concentrate having the potential to be used as a raw material for ironmaking, magnetic separation tailings can be used to solidify metal ions by the sintering method to prepare permeable bricks and comprehensively utilize waste.

4. CONCLUSIONS

Based on the test results and related analysis, the following conclusions can be drawn:

(1) When the pyrolysis temperature is 600 °C, the main reducing components in corncob pyrolysis gas are approximately 4.48 vol % H_2, 0.71 vol % CH_4, and 10.34 vol % CO. According to the thermodynamic analysis, the pyrolysis gas produced by the pyrolysis of corncob at medium and low temperatures has the potential to reduce Fe_3O_2 to Fe_3O_4 in SHPS.

(2) When the reaction temperature is lower than 680 °C, the addition amount of corncob is less than 5%, and the residence time is less than 20 min, the Fe recovery from SHPS increases with increases in these three factors. When the reaction temperature exceeds 680 °C, the addition amount of the corncob is higher than 5%, and the residence time exceeds 20 min, the thorough reduction of SHPS is promoted, and the Fe recovery rate is reduced. With an increase in the magnetic field intensity, the changes in the Fe grade and recovery rate of the product exhibit the opposite trend. In addition, 200 mT is the appropriate magnetic field strength for magnetic separation of the reduction roasted SHPS material. The recovery rate of Fe in SHPS is mainly affected by the temperature, corncob addition ratio, residence time, and magnetic field strength.

(3) Under the optimized conditions (i.e., a reaction temperature of 680 °C, a corncob dosage of 5%, a residence time of 20 min, a roasted product particle size of less than 150 μm, and a magnetic field strength of 200 mT), the recovery rate of Fe reached 91.83%, and the grade of Fe

https://doi.org/10.1021/acsomega.2c01122
ACS Omega 2022, 7, 17963−17975

Figure 14. Photos of the roasted material (a), concentrate (b), and tailings (c).

Table 5. Main Element Contents of the Products after Wet Magnetic Separation (wt %)

project	TFe	SiO_2	Al_2O_3	P	S	$K_2O + Na_2O$	Cl	Ca
concentrate	67.72	1.29	0.11	0.03	0.01	0.01	0.39	1.41
tailings	8.13	32.37	1.58	0.03	0.01	0.13	0.32	22.91

Table 6. Classification of the Magnetite Concentrate Grade[a]

	index (quality score) (%)						
grade	TFe	SiO_2	Al_2O_3	P	S	moisture	granularity
level 1	≥67.0	≤6.0	≤0.8	≤0.05	≤0.08	≤10.0	−0.075 mm: ≥60
level 2	65.0 to <67.0	≤7.0	≤1.0	≤0.10	≤0.12		
level 3	63.0 to <65.0	≤9.0	≤1.2	≤0.10	≤0.20		
level 4	61.0 to <63.0	≤11.0	≤1.2	≤0.10	≤0.20		
level 5	55.0 to <61.0	≤15.0	≤1.5	≤0.10	≤0.50		

[a]Note: the moisture index is for reference.

reached 67.72%, which met the level I requirements in GB/T 32545-2016. Through the verification provided by this experiment, the reducing gas produced by the pyrolysis of corncob can effectively reduce iron oxide in SHPS, allowing this iron oxide to be used as a resource.

AUTHOR INFORMATION

Corresponding Author

Xinqian Shu − *School of Chemistry and Environmental Engineering, China University of Mining and Technology Beijing, Beijing 100083, China;* orcid.org/0000-0002-9023-3195; Email: sxq@cumtb.edu.cn

Authors

Yane Xu − *School of Chemistry and Environmental Engineering, China University of Mining and Technology Beijing, Beijing 100083, China*

Yuanfeng Shu − *School of Chemistry and Environmental Engineering, China University of Mining and Technology Beijing, Beijing 100083, China*

Yichao Wang − *School of Chemistry and Environmental Engineering, China University of Mining and Technology Beijing, Beijing 100083, China*

Xiaoling Ren − *School of Chemistry and Environmental Engineering, China University of Mining and Technology Beijing, Beijing 100083, China*

Xize Zhang − *School of Chemistry and Environmental Engineering, China University of Mining and Technology Beijing, Beijing 100083, China*

Huiyun Song − *School of Chemistry and Environmental Engineering, China University of Mining and Technology Beijing, Beijing 100083, China*

Huixin Zhou − *School of Chemistry and Environmental Engineering, China University of Mining and Technology Beijing, Beijing 100083, China*

Lingwen Dai − *School of Chemistry and Environmental Engineering, China University of Mining and Technology Beijing, Beijing 100083, China*

Zhipu Wang − *State Key Laboratory of Heavy Oil Processing, China University of Petroleum-Beijing at Karamay, Karamay 834000, China*

Xiang Yuan − *Hunan Eijing Drainage Solution Co.Ltd, Changsha 430100, China*

Hongyu Zhao − *Key Laboratory of Coal Processing and Efficient Utilization (Ministry of Education), China University of Mining & Technology, Xuzhou 221116 Jiangsu, China; School of civil and resource engineering, University of Science & Technology Beijing, Beijing 100083, China*

Complete contact information is available at: https://pubs.acs.org/10.1021/acsomega.2c01122

Notes

The authors declare no competing financial interest.

ACKNOWLEDGMENTS

This work was supported by the National Key R&D Plan (2019YFC1904600), the National Natural Science Foundation of China (Grant Nos. 51704016 and 51074170), the State Key Laboratory of Environmental Protection in the Iron and Steel Industry (Grant No. Yzc2017Ky03), the Key Laboratory for Exploration and Comprehensive Utilization of Coal Resources of the Ministry of Land and Resources Open Research Topic (Grant No. KF2016-3), the Xinjiang Uygur Autonomous Region University Scientific Research Plan Project (Grant No.

https://doi.org/10.1021/acsomega.2c01122
ACS Omega 2022, 7, 17963−17975

XJEDU2019Y073), and the Natural Science Foundation of Xinjiang Uygur Autonomous Region (Grant No. 2021D01F37). The authors express their thanks to all of the scientists associated with this article for their encouragement and assistance.

REFERENCES

(1) Liu, T. T.; Zhao, T.; Wang, J.; Huang, Z. C.; Fu, H. H. Generation nodes and disposal status of hazardous wastes from metal surface treatment process. *J. Environ. Eng. Technol.* **2021**, *11*, 1027−1033. (in Chinese)

(2) Xu, Y. E.; Zhang, Y. C.; Shu, Y. F.; Song, H. Y.; Shu, X. Q.; Ma, Y. X.; Hao, L. L.; Zhang, X. Z.; Ren, X. L.; Wang, Z. P.; Zhang, X. L. Composition and Leaching Toxicity of Hydrochloric Acid Pickling Sludge Generated from the Hot-Dip Galvanized Steel Industry. *ACS Omega* **2022**, *7*, 13826−13840.

(3) Fang, B. B.; Chu, Z.; Yang, Y.; Sun, X. Y.; Huang, W. P.; Li, X. F.; Wang, L. J. Characterization of Stainless Steel and Wire Rope Pickling Sludge. *Adv. Mater. Res.* **2013**, *726*−*731*, 2130−2134.

(4) Pinto, F. M.; Pereira, R. A.; Souza, T. M.; Saczk, A. A.; Magriotis, Z. M. Treatment, reuse, leaching characteristics and genotoxicity evaluation of electroplating sludge. *J. Environ. Manage.* **2021**, *280*, No. 111706.

(5) Ministry of Ecology and Environment of the People's Republic of China. *China National List of Hazardous Waste (2021 Version)*. Order No. 15 of the Ministry of Ecology and Environment; Ministry of Ecology and Environment of the People's Republic of China: Beijing, China, 2020.

(6) Mao, L. Q.; Wu, Y. Q.; Zhang, W. Y.; Huang, Q. Q. The reuse of waste glass for enhancement of heavy metals immobilization during the introduction of galvanized sludge in brick manufacturing. *J. Environ. Manage.* **2019**, *231*, 780−787.

(7) Zhang, M. T.; Chen, C.; Mao, L. Q.; Wu, Q. Use of electroplating sludge in production of fired clay bricks: Characterization and environmental risk evaluation. *Constr. Build. Mater.* **2018**, *159*, 27−36.

(8) Zhao, S. Z.; Liu, B.; Ding, Y. J.; Zhang, J. J.; Wen, Q.; Ekberg, C.; Zhang, S. G. Study on glass-ceramics made from MSWI fly ash, pickling sludge and waste glass by one-step process. *J. Cleaner Prod.* **2020**, *271*, No. 122674.

(9) Yang, B.; Jiang, S.; Zhang, C. H.; Zhao, G. F.; Wu, M. M.; Xiao, N.; Su, P. D. Recovery of iron from iron-rich pickling sludge for preparing P-doped polyferric chloride coagulant. *Chemosphere* **2021**, *283*, No. 131216.

(10) Fang, B. J.; Yan, Y.; Yang, Y.; et al. Adsorption of Pb^{2+} from aqueous solution using spinel ferrite prepared from steel pickling sludge. *Water Sci. Technol.* **2016**, *73*, 1112−1121.

(11) Rath, S. S.; Rao, D. S.; Tripathy, A.; Biswal, S. K. Biomass briquette as an alternative reductant for low grade iron ore resources. *Biomass Bioenergy* **2018**, *108*, 447−454.

(12) Wei, R. F.; Li, H. M.; Lin, Y. F.; Yang, L. B.; Long, H. M.; Xu, C. B. C.; Li, J. X. Reduction Characteristics of Iron Oxide by the Hemicellulose, Cellulose, and Lignin Components of Biomass. *Energy Fuels* **2020**, *34*, 8332−8339.

(13) Zhao, H. Y.; Li, Y. H.; Song, Q.; Liu, S. C.; Ma, L.; Shu, X. Q. Catalytic reforming of volatiles from co-pyrolysis of lignite blended with corn straw over three iron ores: Effect of iron ore types on the product distribution, carbon-deposited iron ore reactivity and its mechanism. *Fuel* **2021**, *286*, No. 119398.

(14) Kurniawan, A.; Abe, K.; Nomura, T.; Akiyama, T. Integrated Pyrolysis-Tar Decomposition over Low-Grade Iron Ore for Iron-making Applications: Effects of Coal-Biomass Fuel Blending. *Energy Fuels* **2018**, *32*, 396−405.

(15) Guo, X. S.; Li, Z. Y.; Han, J. C.; Yang, D.; Sun, T. C. Study of Straw Charcoal as Reductant in Co-reduction Roasting of Laterite Ore and Red Mud to Prepare Powdered Ferronickel. *Min., Metall., Explor.* **2021**, *38*, 2217−2228.

(16) Krishnan, M.; Subramanian, H.; Dahms, H. U.; Sivanandham, V.; Seeni, P.; Gopalan, S.; Mahalingam, A.; Rathinam, A. J. Biogenic corrosion inhibitor on mild steel protection in concentrated HCl medium. *Sci. Rep.* **2018**, *8*, No. 2609.

(17) Odewunmi, N. A.; Mazumder, M. A. J.; Ali, S. A.; Aljeaban, N. A.; Alharbi, B. G.; Al-Saadi, A. A.; Obot, I. B. Impact of Degree of Hydrophilicity of Pyridinium Bromide Derivatives on HCl Pickling of X-60 Mild Steel: Experimental and Theoretical Evaluations. *Coatings* **2020**, *10*, 185.

(18) Li, G. H.; Wang, J.; Rao, M. J.; Luo, J.; Zhang, X.; You, J. X.; Peng, Z. W.; Jiang, T. Coprocessing of Stainless-Steel Pickling Sludge with Laterite Ore via Rotary Kiln-Electric Furnace Route: Enhanced Desulfurization and Metal Recovery. *Process Saf. Environ. Prot.* **2020**, *142*, 92−98.

(19) Li, X. M.; Xie, G.; Hojamberdiev, M.; Cui, Y. R.; Zhao, J. X. Characterization and recycling of nickel- and chromium-contained pickling sludge generated in production of stainless steel. *J. Cent. South Univ.* **2014**, *21*, 3241−3246.

(20) Yang, C. C.; Pan, J.; Zhu, D.; Guo, Z. Q.; Li, X. M. Pyrometallurgical recycling of stainless steel pickling sludge: a review. *J. Iron Steel Res. Int.* **2019**, *26*, 547−557.

(21) Kuo, Y.-M. An alternative approach to recovering valuable metals from zinc phosphating sludge. *J. Hazard. Mater.* **2012**, *201*−*202*, 265−272.

(22) Ke, P.; Tian, Y. S.; Cui, J. W. Synergistic effect and product characteristics in microwave co-pyrolysis of lignite and corncob. *Energy Sources, Part A* **2020**, 1−12.

(23) Zheng, A. Q.; Zhao, K.; Li, L. W.; Zhao, Z. L.; Jiang, L. Q.; Zhen, H.; Wei, G. Q.; He, F.; Li, H. B. Quantitative comparison of different chemical pretreatment methods on chemical structure and pyrolysis characteristics of corncobs. *J. Energy Inst.* **2018**, *91*, 676−682.

(24) Wu, Z. Q.; Ma, C.; Jiang, Z.; Luo, Z. Y. Structure evolution and gasification characteristic analysis on co-pyrolysis char from lignocellulosic biomass and two ranks of coal: effect of wheat straw. *Fuel* **2019**, *239*, 180−190.

(25) Song, Q.; Zhao, H. Y.; Jia, J. W.; Yang, L.; Lv, W.; Bao, J. W.; Shu, X. Q.; Gu, Q. X.; Zhang, P. Pyrolysis of municipal solid waste with iron-based additives: A study on the kinetic, product distribution and catalytic mechanisms. *J. Cleaner Prod.* **2020**, *258*, No. 120682.

(26) Yi, S.; He, X. M.; Lin, H. T.; Zheng, H.; Li, C. H.; Li, C. Synergistic effect in low temperature co-pyrolysis of sugarcane bagasse and lignite. *Korean J. Chem. Eng.* **2016**, *33*, 2923−29.

(27) Department of Inorganic Chemistry of Dalian University of Technology. *Inorganic Chemistry*, 5th ed.; Higher Education Press: Beijing, 2006, pp 677−680.

(28) Zhang, Y.; Li, Q.; Liu, X.; Xu, B.; Yang, Y.; Jiang, T. A Thermodynamic Analysis on the Roasting of Pyrite. *Minerals* **2019**, *9*, 220.

(29) Ubando, A. T.; Chen, W. H.; Ong, H. C. Iron oxide reduction by graphite and torrefied biomass analyzed by TG-FTIR for mitigating CO_2 emissions. *Energy* **2019**, *180*, 968−977.

(30) Sohn, I.; Fruehan, R. J. The reduction of iron oxides by volatiles in a rotary hearth furnace process: Part II. The reduction of iron oxide/carbon composites. *Metall. Mater. Trans. B* **2006**, *37*, 223−229.

(31) Kobayashi, N.; Itaya, Y. Performance of Iron Oxide-Based Oxygen Carrier in Biomass Pyrolysis. *J. Chem. Eng. Jpn.* **2018**, *51*, 469−475.

(32) Ding, D. J.; Peng, H.; Peng, W. J.; Yu, Y. W.; Wu, G. X.; Zhang, J. Y. Isothermal hydrogen reduction of oxide scale on hot-rolled steel strip in 30 pct H_2−N_2 atmosphere. *Int. J. Hydrogen Energy* **2017**, *42*, 29921−29928.

(33) Wang, Y. C.; Luo, G. P.; Bai, J. B.; Wu, H. L. Study on influence of F, K and Na on solid phase reaction of sintering process. *Iron Steel* **2008**, *7*, 12−15. (in Chinese)

(34) Kamijo, C.; Hoshi, M.; Kawaguchi, T.; Yamaoka, H.; Kamei, Y. Production of direct reduced iron by a sheet material inserting metallization method. *ISIJ Int.* **2001**, *41*, S13−S16.

(35) Song, Q.; Zhao, H. Y.; Jia, J. W.; Zhang, F.; Wang, Z. P.; Lv, W.; Yang, L.; Zhang, W.; Zhang, Yi.; Shu, X. Q. Characterization of the products obtained by pyrolysis of oil sludge with steel slag in a

https://doi.org/10.1021/acsomega.2c01122
ACS Omega 2022, 7, 17963−17975

continuous pyrolysis-magnetic separation reactor. *Fuel* **2019**, *255*, No. 115711.
(36) Guo, D. B.; Hu, M.; Pu, C. X.; Xiao, B.; Hu, Z. O.; Liu, S. M.; Wang, X.; Zhu, X. L. Kinetics and mechanisms of direct reduction of iron ore-biomass composite pellets with hydrogen gas. *Int. J. Hydrogen Energy* **2015**, *40*, 4733−4740.
(37) Standardization Administration Committee of the People's Republic of China. *Division of Production Grade for Iron Ores*, Chinese Standard GB/T 32545-2016; Standardization Administration Committee of the People's Republic of China: Beijing, China, 2016.

https://doi.org/10.1021/acsomega.2c01122
ACS Omega 2022, 7, 17963−17975